



Oxygen Reduction Reaction Activity of Microwave Mediated Solvothermal Synthesized CeO₂/g-C₃N₄ Nanocomposite

Siba Soren¹, Ipsha Hota¹, A. K. Debnath², D. K. Aswal², K. S. K. Varadwaj¹ and Purnendu Parhi^{1*}

¹ Department of Chemistry, Ravenshaw University, Cuttack, India, ² Technical Physics Division, Bhabha Atomic Research Center, Mumbai, India

OPEN ACCESS

Edited by:

Zhong Jin,
Nanjing University, China

Reviewed by:

Mahmut Özacar,
Sakarya University, Turkey
Hongjie Zhang,
Changchun University of Science and
Technology, China

*Correspondence:

Purnendu Parhi
pparhi@ravenshawuniversity.ac.in

Specialty section:

This article was submitted to
Inorganic Chemistry,
a section of the journal
Frontiers in Chemistry

Received: 22 February 2019

Accepted: 20 May 2019

Published: 06 June 2019

Citation:

Soren S, Hota I, Debnath AK,
Aswal DK, Varadwaj KSK and Parhi P
(2019) Oxygen Reduction Reaction
Activity of Microwave Mediated
Solvothermal Synthesized
CeO₂/g-C₃N₄ Nanocomposite.
Front. Chem. 7:403.
doi: 10.3389/fchem.2019.00403

Electrocatalytic active species like transition metal oxides have been widely combined with carbon-based nanomaterials for enhanced Oxygen Reduction Reaction (ORR) studies because of the synergistic effect arising between different components. The aim of the present study is to synthesize CeO₂/g-C₃N₄ system and compare the ORR activity with bare CeO₂. Ceria (CeO₂) embedded on g-C₃N₄ nanocomposite was synthesized by a single-step microwave-mediated solvothermal method. This cerium oxide-based nanocomposite displays enhanced ORR activity and electrochemical stability as compared to bare ceria.

Keywords: g-C₃N₄, CeO₂, cyclic voltammogram, linear sweep voltammetry, rotating disk electrode, rotating ring disk electrode

INTRODUCTION

Metal-air batteries and fuel cells are alternative energy transfer devices designed to meet the requirements of sustainable energy (Sun et al., 2017). Direct Methanol Fuel Cells (DMFCs) are documented as an ideal candidate for laptop, mobile, and digital camera applications. Efficient reduction of O₂ to water is a major challenge in energy conversion in DMFCs. The Oxygen Reduction Reaction (ORR) in alkaline DMFCs proceeds via a 4-electron pathway, (O₂ + 2H₂O + 4e⁻ → 4OH⁻) which is preferable over the 2-electron pathway (O₂ + H₂O + 2e⁻ → HO₂⁻ + OH⁻) (Zhang and Song, 2008). The 2-electron process is unfavorable because of the production of corrosive peroxide species, which can cause degradation of electrochemical cells. The precious metal catalysts such as Pt and Pt-based alloys used to catalyze the ORR process are expensive and available in limited quantity (Peng and Yang, 2009; Kim et al., 2010). These Pt-based catalysts are also intolerant to methanol, which is used as fuel in DMFCs. Design of new non-precious electrocatalyst with improved ORR activity is still a challenge before the scientific community. First row transition metal oxides (TMOs) (Bashyam and Zelenay, 2006; Cheng et al., 2009; Jaouen et al., 2011; Cheng and Chen, 2012) have already been used as robust alternatives for promoting the ORR in alkaline conditions. The low electrical conductivity of the TMOs influences the electron transfer process in ORR (Soren et al., 2016).

Carbon materials possess a specific place for the ORR in DMFCs. Various carbon materials like graphite (Jiao et al., 2014), carbon black, carbon nanotube, and activated carbon are mostly used as supporting materials in the preparation of electrocatalysts due to their high electrical conductivity, corrosion resistance, porous structure and specific surface area (Liang et al., 2011). TMOs when

embedded with reduced graphene oxide show enhanced catalytic performance because of a synergetic effect between TMOs and graphene oxide (Liang et al., 2011, 2012; Wang et al., 2011; Guo and Sun, 2012; Guo et al., 2012; Wu et al., 2015).

Hetero atoms (e.g., N, B, P, S, and I) were also doped in the reduced graphene oxide in order to improve the catalytic active sites in reduced graphene oxide (Behnam, 2017). In the recent past, nitrogen-doped graphene oxide has become a potential carbon-based electrocatalyst for ORR because of its low cost, high stability, and high efficiency (Qu et al., 2010; Geng et al., 2011; Yang et al., 2012; Paraknowitsch and Thomas, 2013). The electronic environment of doping nitrogen on a reduced graphene sheet in three configurations (e.g., pyridinic, pyrrolic, and graphitic nitrogen) induces an uneven charge distribution in adjacent sites, and as a result it alters the local spin or charge density. It promotes oxygen adsorption and helps in the enhancement of ORR performance (Ikeda et al., 2008; Niwa et al., 2009; Liu et al., 2010; Qu et al., 2010; Rao et al., 2010; Kim et al., 2011; Li et al., 2011, 2013; Sheng et al., 2011; Zhang and Xia, 2011; Lai et al., 2012; Parvez et al., 2012; Sharifi et al., 2012; Wang et al., 2012; Zhang et al., 2013; Zheng et al., 2013; Bag et al., 2014). Transition metal oxide embedded in N doped carbon systems is reported as a promoter of ORR catalytic activity by facilitating electron transfer (Bag et al., 2014). Rare earth oxide-based systems are now extensively studied for ORR due to their unique electronic structure, bonding characteristics and variable oxidation states. There are very few reports available in the literature where rare earth oxides such as lanthanum oxide, samarium oxide, and cerium oxide have been studied for their ORR properties (Soren et al., 2016; Wang et al., 2016, 2017). The unique structural properties of CeO₂ have contributed toward the promising electrocatalytic activity of CeO₂. However, poor electronic conductivity of CeO₂ limits its application toward ORR. Thus, in order to enhance the electrocatalytic activity, CeO₂ is doped with different metals or embedded with a conductive active framework. Recently, our group has published an article on ORR activity of the CeO₂/NrGO system (Soren et al., 2016).

Researchers have found a new material analogy to N-doped rGO called graphitic carbon nitride (g-C₃N₄) (Qiao et al., 2016). It is a carbon- and nitrogen-based polymeric material. Graphitic carbon nitride (g-C₃N₄) is a nitrogen-rich carbon-based material. But as reported in the literature g-C₃N₄ is an inert electrocatalyst (Liu and Zhang, 2013; Zou et al., 2013). However, g-C₃N₄ with metal doping or metal oxide doping has already been reported as a promising electrocatalyst for ORR and OER (Oxygen Evolution Reaction), when embedded with transition metal/metal oxide (Liu and Zhang, 2013; Zou et al., 2013).

It is expected that CeO₂/g-C₃N₄ composite can enhance the ORR in fuel cells. In this paper, we have investigated the ORR activity of CeO₂ embedded with g-C₃N₄ to show whether it follows a 2-electron or 4-electron pathway in the ORR process. The hybrid CeO₂/g-C₃N₄ nanostructures were prepared by the microwave mediated polyol method.

MATERIALS AND METHODS

Chemicals

Melamine, Ammonium Cerium (IV) Nitrate and 1, 4-Butanediol were procured from HIMEDIA. All the chemicals were used as received.

Synthesis of g-C₃N₄

About 3 g of melamine was taken in china crucible and was heated for 4 h at 520°C with a moderate heating rate of 10°C/min inside the muffle furnace. The product obtained was cooled to room temperature. The prepared g-C₃N₄ was characterized for further work.

Synthesis of CeO₂/g-C₃N₄ Composite

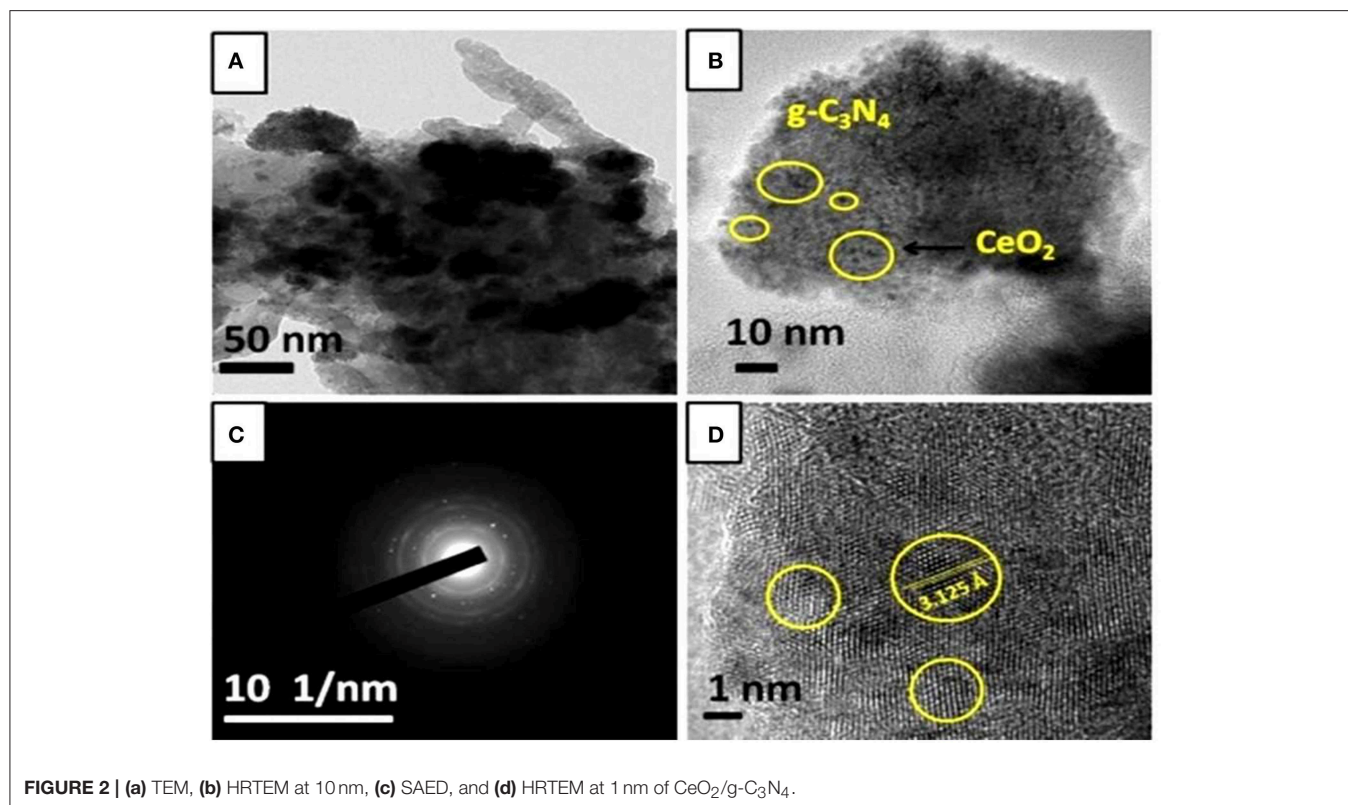
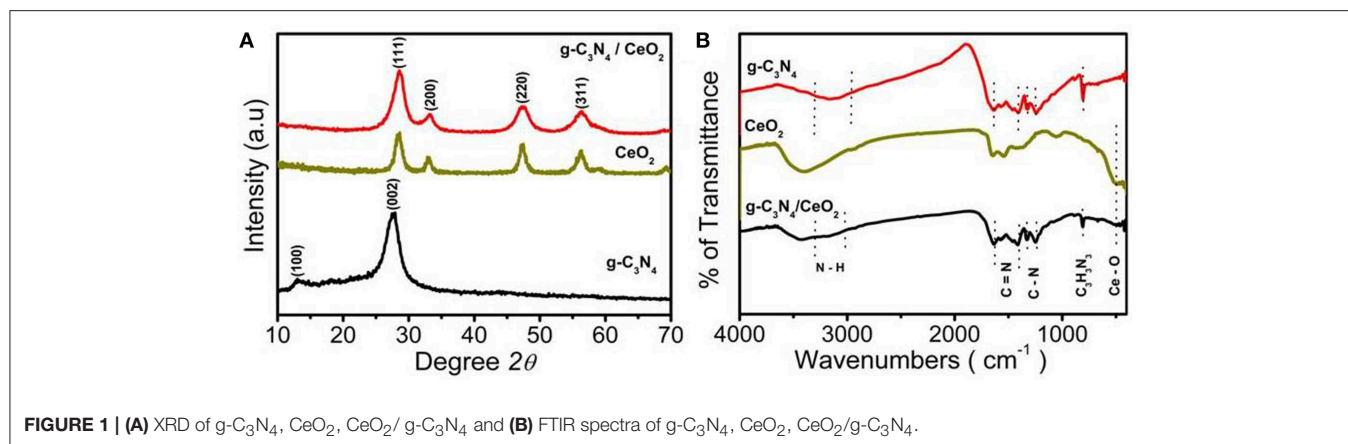
In typical synthesis 50 mg of the above-prepared g-C₃N₄ was added to 20 ml of 1, 4-butanediol. The solution was stirred at 300 rpm in a 50 ml beaker to make a heterogeneous mixture. A total of 250 mg of ammonium cerium (IV) nitrate was added to this heterogeneous solution and again stirred at the same rpm for 10 min until the color of the solution changed from light yellow to orange red. The entire solution was transferred to a Teflon vessel. The vessel was tightly sealed and irradiated with microwave radiation (MDS 6) for 10 min at 180°C. The reaction mixture was allowed to cool to room temperature after completion of the reaction. The obtained light yellow-colored precipitate was centrifuged several times with distilled water, ethanol, and acetone to remove the impurities. Finally, the product was kept for drying in an oven over night at 60°C.

Characterization

The crystallographic phases were identified by XRD measurements using a Rigaku Ultima-IV Advance X-ray Diffractometer operating at 40 KV (radiation source Cu K α , wavelength = 1.5418 Å). FTIR analysis was carried out with the help of Thermo Fischer Nicolet iS5 FTIR instrument. The XPS measurement was performed using DESA-150 electron analyzer (Staub (1253.6 eV) as radiation source. Transmission Electron Microscope (TEM) and High Resolution Transmission Electron Microscope (HRTEM) images were obtained by the Model FEI Technai G2 S-Twin (Benson et al., 2014). Electrochemical Impedance Spectroscopic analysis was recorded CH660E electrochemical work station.

Electrochemical Measurements

The electrochemical measurements were conducted in a conventional three-electrode system using a Metrohm Autolab 204 B.V. (Metrohm Autolab, Netherland). During the measurements, saturated Ag/AgCl electrode, Pt wire, and modified glassy carbon (GC) electrode were used as reference, counter, and working electrode respectively. Synthesized electrocatalyst material was loaded on a pre-cleaned GC electrode during preparation of the working electrode. For the preparation of catalytic ink 5 mg of as synthesized electrocatalyst was dispersed in 2 ml isopropanol, 3 ml double distilled H₂O, and 25 micro liter Nafion solution (as binder) in an ultrasonic bath for 30 min (Soren et al., 2016). About 12 μ l of well-dispersed catalytic ink (~0.012 mg) was drop casted onto the polished GC



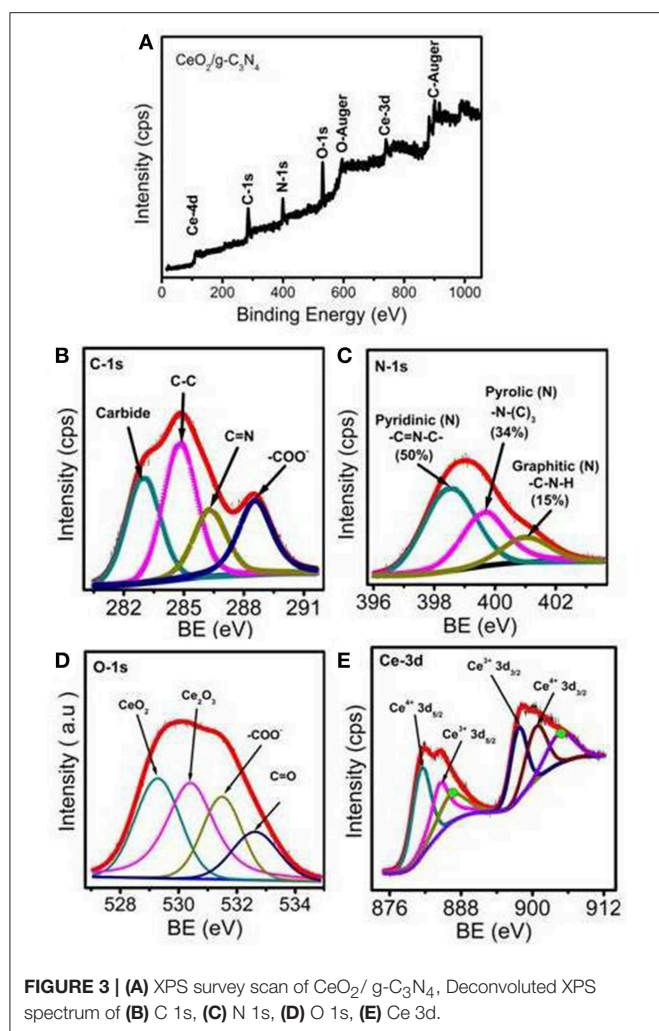
electrode of surface area (0.07067 cm²). The modified glassy carbon electrode was dried in a vacuum oven for 3 h. About 33.3 μl of previously prepared catalyst ink was drop casted on RRDE electrode (GC disk electrode) with 5 mm diameter ($S = 0.196$ cm²) to make the loading the same as in RDE studies.

RESULT AND DISCUSSION

Composition and Structure Characterization of CeO₂/gC₃N₄ Hybrid

XRD patterns of the synthesized composite (1:1) were studied and compared with the XRD pattern of individual CeO₂ and g-C₃N₄ (Ferrero et al., 2016). In the case of a pure g-C₃N₄ sample,

a strong diffraction peak appears at 27.61° that corresponds to the (002) plane. The strong diffraction peak arises because of the stacking of the conjugated aromatic system (Wang et al., 2009). The sharp peak at 27.61° indicates tight packing in g-C₃N₄, which is because of the strong binding between the layers and large localization of electrons. Another small peak at 13.12° can be assigned to the (100) plane. The diffraction peaks of the pure cubic fluorite structure of CeO₂ were indexed to the (111), (200), (220), and (311) planes (JCPDS 81-0792) (Soren et al., 2015). After the incorporation of CeO₂ into the g-C₃N₄ network, the XRD pattern shows an absence of peak at 13.12° even though the weight ratio of g-C₃N₄ and CeO₂ are nearly 1:1 in the composite (Liu and Zhang, 2013). The peak corresponding to the (111) plane of CeO₂, which coincides with the highest intensity peak of



bare g-C₃N₄, has been shifted to higher 2θ value, and the intensity of the peak has also been increased. From these findings it can be concluded that CeO₂ nanoparticles are successfully embedded into in-planes of g-C₃N₄ sheets (Thomas et al., 2008; Zhang et al., 2008; Xu et al., 2013) (Figure 1A).

The chemical structures of the samples were evaluated by the FTIR analysis. A broad band between 3,000 and 3,500 cm⁻¹ was noticed in the composite, which can be attributed to stretching vibration of N-H and surface adsorbed water molecules. The absorption peaks at 1,572 and 1,632 cm⁻¹ (Li et al., 2015) were due to C=N stretching (Bojdyts et al., 2008; Yan et al., 2009) while for aromatic C-N stretching, peaks at 1,253, 1,320, and 1,425 cm⁻¹ were observed. The main structural peaks at 808 cm⁻¹ corresponded to the breathing mode of triazine units of g-C₃N₄ (Xu et al., 2013), which reveals that the graphitic C-N network of g-C₃N₄ was not affected even after the inclusion of CeO₂ in the g-C₃N₄ layer (Figure 1B).

CeO₂/g-C₃N₄ composite showed a layered structure of g-C₃N₄ (Figure 2a), and several small dark images of CeO₂ nanoparticle appeared in the TEM image

(Figure 2b). The appearance of some bright spots and the diffuse rings in the SAED pattern of CeO₂/g-C₃N₄ corresponds to the growth of crystalline CeO₂ nanoparticle on the amorphous g-C₃N₄ sheet (Figure 2c). The fringe spacing was measured to be 3.125 Å, which corresponds to the (111) lattice plane of the cubic fluorite CeO₂ structure (Figure 2d).

The composition and chemical structure of the synthesized material were established by X-ray photoelectron spectroscopy. The high resolution XPS survey spectra of C 1s, N 1s, O 1s, and Ce 3d XPS spectra of CeO₂/g-C₃N₄ (1:1) composite is shown in Figure 3A. The XPS spectra of the C 1s core level for CeO₂/g-C₃N₄ can be deconvoluted into four components including the standard reference carbon (283 eV) (Xing et al., 2014). The peak at 284.8 eV corresponds to sp²-bonded C-C (Raymundo-Pinero et al., 2002). The peaks at 286.3 and 288.5 eV (Guan et al., 2018) are ascribed to C=N and N-C-N in g-C₃N₄ respectively (Figure 3B) (Yan et al., 2012). The main peak of N 1s at 398.5 eV is assigned to sp² nitrogen (C=N-C) (pyridinic) present in triazine rings, while the peak at 399.6 eV arises from the tertiary nitrogen bonded to carbon atoms in the form of N-(C)₃ (pyrrolic). The peak at 401.1 eV can be ascribed to g (C-N-H) (graphitic) (Figure 3C) (Raymundo-Pinero et al., 2002). The % of N in total spectrum is calculated to be 7.09%. The percentages of different levels of nitrogen in the system were 50.6, 34.48, and 15.05% for pyridinic, pyrrolic, and graphitic nitrogen, respectively. The O 1s spectrum is deconvoluted at 529.2, 531.0, and 533.2 eV for CeO₂, COOH and OH respectively. These spectra suggest the formation of CeO₂ on g-C₃N₄ (Figure 3D). The oxidation states of Ce in g-C₃N₄/CeO₂ composites were examined by deconvolution of Ce 3d peaks. The two peaks at 881.6 and 884.7 eV can be attributed to 3d_{5/2} of Ce⁴⁺ and Ce³⁺ core electrons respectively. Further peaks at 897.5 and 900.1 eV can be ascribed to 3d_{3/2} of Ce³⁺ and Ce⁴⁺, respectively (Figure 3E) (Zheng et al., 2017).

Electrochemical Performance of CeO₂/gC₃N₄ Hybrid

The cyclic voltammogram (CV) was performed in N₂ as well as O₂ saturated 0.1 M KOH solution for the three materials (g-C₃N₄, CeO₂ and CeO₂/g-C₃N₄) in the potential range of -0.8 to 0.2 V at various scan rates (Ferrero et al., 2016). No reduction peaks were observed in the N₂-saturated condition. After O₂ was introduced for 30 min, intense reduction peaks of g-C₃N₄ (Jiao et al., 2014), CeO₂, and CeO₂/g-C₃N₄ at E_{onset} -0.3, -0.24, and -0.17 V vs. Ag/AgCl, respectively, were recorded (Figure 4A). To investigate ORR performance, linear sweep voltammetry (LSV) was recorded for the prepared materials together with commercial 20 wt% Pt/C, in O₂ saturated 0.1 M KOH solution using Rotating Disk Electrode (RDE) at 1,600 RPM (Wu X. et al., 2017). From the LSV, plot the onset potential was observed to be -0.3, -0.23, and -0.2 V vs. Ag/AgCl for g-C₃N₄, CeO₂, and CeO₂/g-C₃N₄, respectively (Figure 4B). The shift in onset potential of 30 mV for CeO₂/g-C₃N₄ as compared to CeO₂ indicates a synergistic interaction between CeO₂ and g-C₃N₄ in

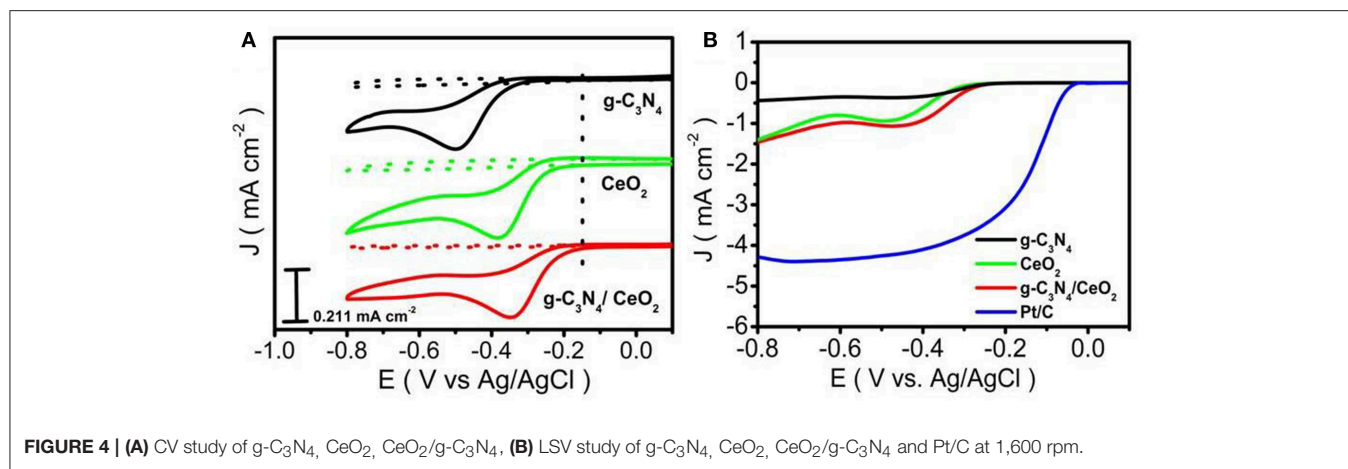


FIGURE 4 | (A) CV study of g-C₃N₄, CeO₂, CeO₂/g-C₃N₄, **(B)** LSV study of g-C₃N₄, CeO₂, CeO₂/g-C₃N₄ and Pt/C at 1,600 rpm.

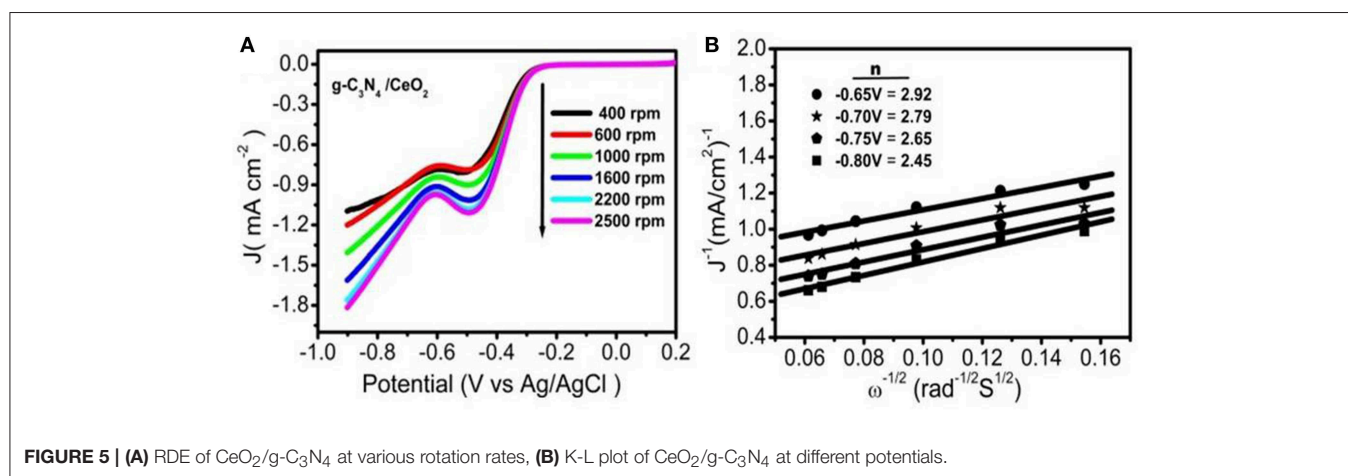


FIGURE 5 | (A) RDE of CeO₂/g-C₃N₄ at various rotation rates, **(B)** K-L plot of CeO₂/g-C₃N₄ at different potentials.

the composite which facilitates ORR, but the constancy in the current value of CeO₂/g-C₃N₄ composite with CeO₂ indicates a slow ORR rate. A positive shift of onset potential (100 mV) between CeO₂/g-C₃N₄ ($E_{\text{onset}} = -0.2\text{V}$ vs. Ag/AgCl) and g-C₃N₄ ($E_{\text{onset}} = -0.3\text{V}$ vs. Ag/AgCl) suggests a strong interaction between CeO₂ and g-C₃N₄. We observed a small improvement in the $E_{1/2}$ for CeO₂/g-C₃N₄ composite ($E_{1/2}$ is -0.383V) as compared to their individual counterparts ($E_{1/2}$ is -0.383V and -0.388V for bare CeO₂ and g-C₃N₄, respectively) (Ferrero et al., 2016). LSVs of CeO₂/g-C₃N₄ at different rotation speeds from 400 to 2,500 rpm were carried out with Rotating Disk Electrode (RDE) to study electron transfer kinetics during ORR process (Figure 5A). It is observed that with an increase in rotation rate the diffusion rate of oxygen molecules also increases, which leads to a gradual increase in current density value. Koutecky–Levich (K–L) plots were plotted (Figure 5B) in order to gain better insight into the electron transfer process during ORR. The Koutecky–Levich (K–L) equation is given as follows:

$$1/J = 1/J_L + 1/J_K = (1/B)\omega^{-1/2} + 1/J_K \quad (1)$$

$$B = 0.62nFC_0(D_0)^{2/3}\nu^{1/6} \quad (2)$$

Here J is the measured current density, J_L and J_K are the diffusion and kinetic current densities, respectively, n is the transferred electron number per O₂ molecule, ω is the angular velocity, F is the Faraday constant ($F = 96,485\text{C mol}^{-1}$), D_0 is the O₂ diffusion coefficient ($1.9 \times 10^{-5}\text{cm}^2\text{s}^{-1}$), C_0 is the bulk concentration of O₂ ($1.2 \times 10^{-3}\text{mol L}^{-1}$), ν is the kinematic viscosity of the electrolyte ($0.01\text{m}^2\text{s}^{-1}$) (Soren et al., 2016). At various electrode potentials J^{-1} vs. $\omega^{-1/2}$ graphs were plotted for CeO₂/g-C₃N₄ (Figure 5B). The number of electrons transferred per O₂ molecule (n) was calculated from the slopes of the best fit lines (Soren et al., 2016). The n value for the CeO₂/g-C₃N₄ nanocomposite was calculated around 3, which suggests the ORR kinetics proceeds through the 2-electron pathway.

To gain more information on the ORR mechanism, the electron transfer number ' n ' and the rate of peroxide formation can be determined from the RRDE analysis (Ge et al., 2015). In RRDE, the ORR takes place at the GC disk (where the different catalysts were deposited) and the concentric Pt ring detects the peroxide production. Figure 6 shows the disk and ring currents for the CeO₂ and CeO₂/g-C₃N₄ systems. Both catalysts generate ring current at the onset potential for the ORR. All three electrodes display large disk currents with relatively low ring current. Here, n is the

number of electrons transferred, I_D is the current measured at the GC disk, and I_R is the current measured at the Pt ring obtained through RRDE (Qiao et al., 2016). The value of “ N ” is 0.25, denoting the collection efficiency which is a design parameter provided by the RRDE manufacturer. The following two equations are used to determine electron transfer number and amount of peroxide produced during ORR (Ge et al., 2015).

$$n = \frac{4I_D}{I_D + (I_R/N)} \quad (3)$$

$$\%HO_2^- = \frac{200(I_R/N)}{I_D + (I_R/N)} \quad (4)$$

At lower over potential regions ($-0.4V$ vs. Ag/AgCl), the average value of “ n ” for CeO₂, CeO₂/g-C₃N₄ were 2.71, 3.2, respectively. The peroxide formation follows the reverse trend (CeO₂ > CeO₂/g-C₃N₄). At higher over potential regions ($-0.6V$ vs. Ag/AgCl) the “ n ” of CeO₂ and CeO₂/g-C₃N₄ remains constant, i.e., 2.57 and 3.2 respectively (Figure 7A). This indicates at the quasi-4-electron process followed CeO₂/g-C₃N₄. The peroxide

formation follows the reverse trend (CeO₂ > CeO₂/g-C₃N₄) at higher over potential regions (Figure 7B).

An enhancement of reaction kinetics toward the 4-electron ORR pathway is clearly observed from CeO₂ to CeO₂/g-C₃N₄. The ORR activity can be ascribed to the oxygen vacancies in the CeO₂ lattice, which originated from the mixed valence states. The defects can be easily healed by oxygen adsorption when exposed to oxygen environment (Soren et al., 2016). The improved ORR activity of CeO₂/g-C₃N₄ can be explained by considering the synergistic effect between CeO₂ and carbon network containing different types of nitrogen (Pyridinic, pyrolic, and graphitic). Ruoff's group in their recent publication has confirmed the effect of nitrogen doping on the ORR activity (Lai et al., 2012). They have concluded that the catalytic activity is dependent on the nature and amount of nitrogen present in the matrix. It has been established that presence of graphitic nitrogen increases the limiting current whereas the pyridinic nitrogen alters the onset potential of ORR (Soren et al., 2016). Li et al. have shown that the direct reduction pathway for ORR is favored by the presence of pyridinic nitrogen (Li et al., 2013). Bag et al. also confirmed the vital role of pyridinic nitrogen in the enhancement of ORR activity (Bag et al., 2014). In this paper the XPS analysis reveals that CeO₂/g-C₃N₄ has 50.6% pyridinic nitrogen. This explains the shift in onset potential while going from CeO₂ to CeO₂/g-C₃N₄ composite (as discussed in Figure 4B)

Stability of electrocatalysts is another key parameter in the evaluation of their catalytic performance. The catalytic stability of CeO₂/g-C₃N₄ along with commercial Pt/C and bare CeO₂ were measured and compared by the Chronoamperometric response method at $-0.35V$ vs. Ag/AgCl in 0.1M KOH solution for 12,500 s at 1,000 rpm, and the results are shown in Figure 8 (Soren et al., 2016). As expected, CeO₂/g-C₃N₄ exhibited better stability as compared to both Pt/C as well as bare CeO₂. Moreover, after 12,500 s, relative current value for bare CeO₂ and Pt/C decreased by 53 and 40% respectively, while in case of CeO₂/g-C₃N₄ composite a 24% decrease in the relative current was observed.

Methanol poisoning of the cathode impacts the ORR process. As a result, it is very much essential to address another important

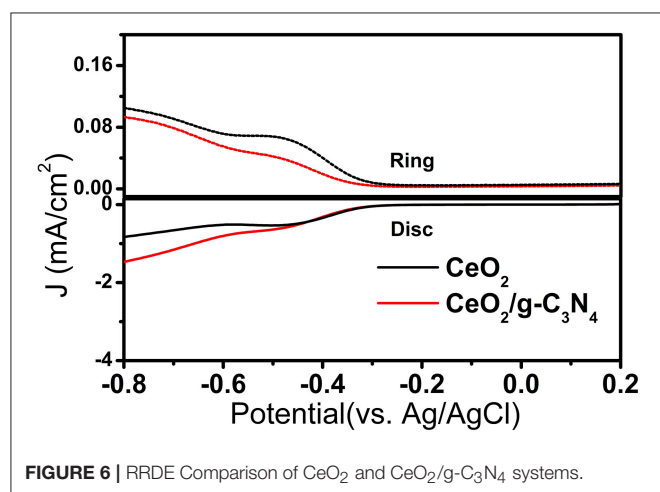


FIGURE 6 | RRDE Comparison of CeO₂ and CeO₂/g-C₃N₄ systems.

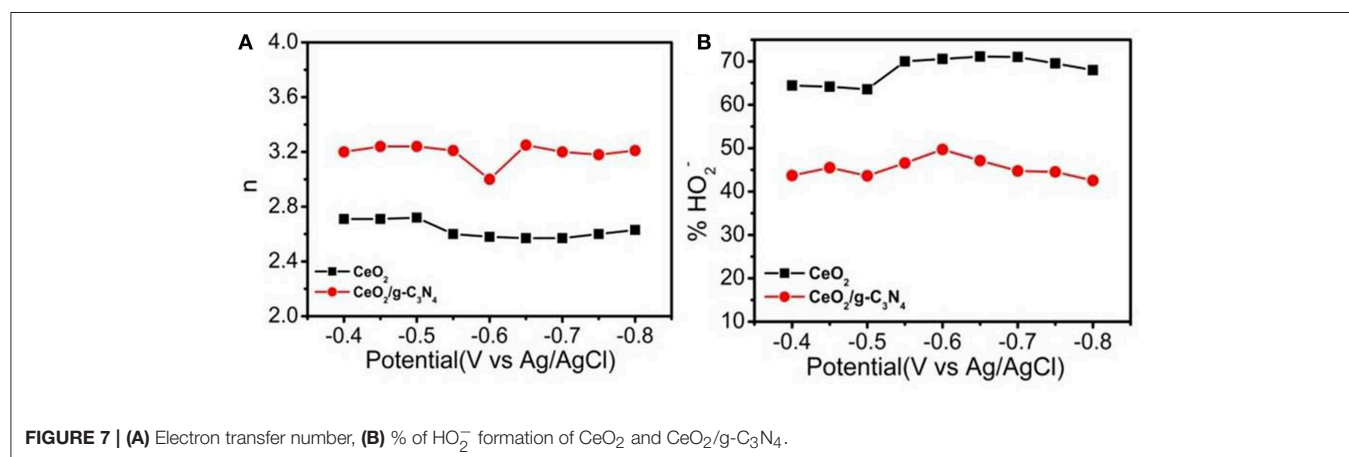
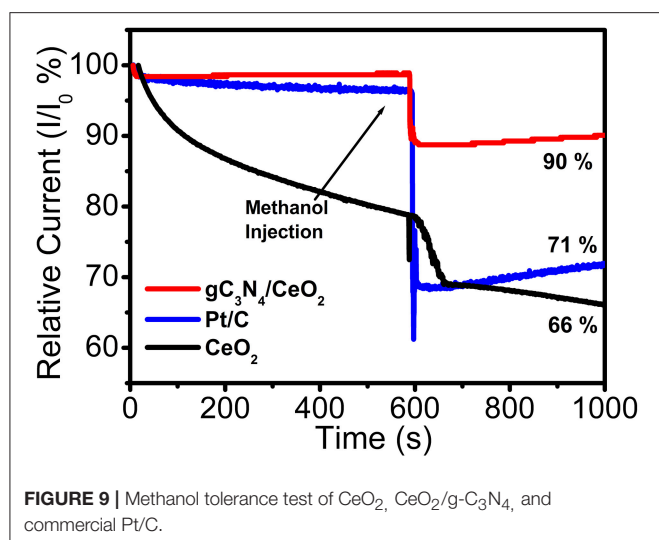
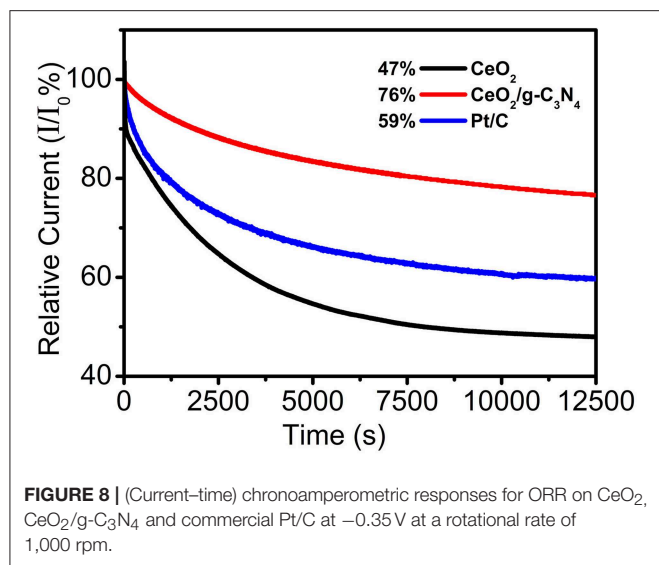


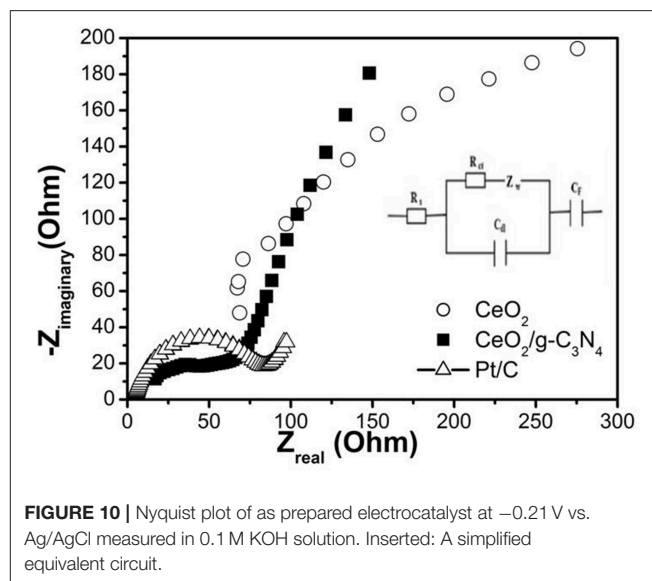
FIGURE 7 | (A) Electron transfer number, (B) % of HO₂⁻ formation of CeO₂ and CeO₂/g-C₃N₄.



factor of ORR catalysis—i.e., methanol tolerant capability (Bag et al., 2014). For methanol tolerance, test chronoamperometric measurements were performed at -0.35 V vs. Ag/AgCl at 1,000 rpm in O₂ saturated 0.1 M KOH solution to investigate the methanol crossover effect of CeO₂, CeO₂/g-C₃N₄ composite as well as of commercial Pt/C. A total of 25 mL of (10 wt%) 3 M methanol was injected at 600 s. It was observed that there was a 34% and 29% decrease in relative current for CeO₂, Pt/C, respectively, whereas only a 10% decrease in relative current was observed for the CeO₂/g-C₃N₄ composite system (Figure 9). This result demonstrates the better methanol tolerance ability of CeO₂/g-C₃N₄ as compared to Pt/C.

Impedance Measurement

Electrochemical impedance spectroscopy (EIS) is another potent technique to describe the electrocatalyst kinetics and interface properties in ORR (Perini et al., 2015). EIS analysis



through Nyquist plots is generally used to examine interfacial charge transport behavior of the electrode-electrolyte interface. The Nyquist plots demonstrate variation of impedance with frequency reflected as imaginary component vs. real component of impedance. Figure 10 shows the Nyquist plots over the frequency range 100–1 MHz for the CeO₂/g-C₃N₄ modified electrode in 0.1 M KOH solution with an AC amplitude of 0.1 V at an initial potential of -0.210 V. The Nyquist plot is represented at high frequency by a semicircular arc and at low frequency the plot is represented by a straight line. In this plot, the charge transfer resistance at the electrode-electrolyte interface is represented by the diameter of the semicircular arc whereas the diffusion nature of the electrolyte at the electrode surface is represented by a straight line (Parwaiz et al., 2017). The impedance data was fitted to an equivalent circuit (inset of Figure 10). The equivalent circuit consists of charge transfer resistance (R_{ct}), solution resistance (R_s), pseudocapacitance (C_F), Warburg impedance (Z_w), and double layer capacitance (C_{dl}) (Tan and Ren, 2016). The semicircle intercepting the real axis is a combination of both charge transfer resistance R_{ct} (Guan et al., 2018) and ionic resistance of electrolyte R_s (Maheswari and Muralidharan, 2016). R_s consists of bulk electrolyte solution resistance and electron transfer resistance whereas R_{ct} can be ascribed to charge transfer resistance at the electrode-electrolyte boundary (Maheswari and Muralidharan, 2015).

The calculated R_s for the CeO₂/g-C₃N₄ composite is 36.5 Ω . The value of R_s of the electrodes can be attributed to the dissimilar conductivities and morphologies of the materials in their construction. A faster electron-transfer rate can be designated by a smaller R_{ct} (Wu Q. et al., 2017). Based on the observations, the diameter of the semicircle and the calculated R_{ct} of the CeO₂/g-C₃N₄ is 150 Ω whereas the R_{ct} for CeO₂ and Pt/C was found to be 534.4 and 77.3 Ω , respectively. The lower R_{ct} value of CeO₂/g-C₃N₄ can be assigned to active electron transfer kinetics which in turn favor ORR catalytic activity.

CONCLUSION

In accordance with the study report, CeO₂/g-C₃N₄ was successfully synthesized by a facile microwave mediated polyol route. The synergic effect of CeO₂ after interacting g-C₃N₄ leads to the enhancement of ORR activity of the CeO₂/g-C₃N₄ modified system as compared to bare CeO₂. The XPS and ORR kinetics study results reveal that CeO₂/g-C₃N₄ with high levels of pyridinic nitrogen performs better ORR catalytic activity, implying a vital role of pyridinic nitrogen as promoter of ORR. The composites have shown excellent ORR stability and methanol tolerance behavior than commercial Pt/C. The low cost and facile synthesis procedure predict the future utility of the CeO₂/g-C₃N₄ composite in energy conversion system.

REFERENCES

- Bag, S., Roy, K., Gopinath, C. S., and Raj, C. R. (2014). Facile single-step synthesis of nitrogen-doped reduced graphene oxide-Mn₃O₄ hybrid functional material for the electrocatalytic reduction of oxygen. *ACS Appl. Mater. Interf.* 6, 2692–2699. doi: 10.1021/am405213z
- Bashyam, R., and Zelenay, P. (2006). A class of non-precious metal composite catalysts for fuel cells. *Nat. Lett.* 443, 63–66. doi: 10.1038/nature05118
- Behnam, S. (2017). Bio-inspired iron metal-carbon black based nano-electrocatalyst for the oxygen reduction reaction. *Pigment Resin Technol.* 46, 267–275. doi: 10.1108/PRT-07-2016-0081
- Benson, J., Xu, Q., Wang, P., Shen, Y., Sun, L., Wang, T., et al. (2014). Tuning the catalytic activity of graphene nanosheets for oxygen reduction reaction via size and thickness reduction. *ACS Appl. Mater. Interf.* 6, 19726–19736. doi: 10.1021/am5048202
- Bojdys, M. J., Muller, J. O., Antonietti, M., and Thomas, A. (2008). Ionothermal synthesis of crystalline, condensed, graphitic carbon nitride. *Chem. Eur. J.* 14, 8177–8182. doi: 10.1002/chem.200800190
- Cheng, F., and Chen, J. (2012). Metal-air batteries: from oxygen reduction electrochemistry to cathode catalysts. *Chem. Soc. Rev.* 41, 2172–2192. doi: 10.1039/c1cs15228a
- Cheng, F., Shen, J., Ji, W., Tao, Z., and Chen, J. (2009). Selective synthesis of manganese oxide nanostructures for electrocatalytic oxygen reduction. *ACS Appl. Mater. Interf.* 2, 460–466. doi: 10.1021/am800131v
- Ferrero, G. A., Antonio, B. F., Marta, S., and Maria-Magdalena, T. (2016). Efficient metal-free N-doped mesoporous carbon catalysts for ORR by a template-free approach. *Carbon* 106, 179–187. doi: 10.1016/j.carbon.2016.04.080
- Ge, X., Sumboja, A., Wu, D., Wu, T., An, T., Li, B., et al. (2015). Oxygen reduction in alkaline media: from mechanisms to recent advances of catalysts. *ACS Catal.* 5, 4643–4667. doi: 10.1021/acscatal.5b00524
- Geng, D., Chen, Y., Li, Y., Li, R., Sun, X., Ye, S., et al. (2011). High oxygen-reduction activity and durability of nitrogen-doped graphene. *Energ. Environ. Sci.* 4, 11760–11764. doi: 10.1039/c1ee00326c
- Guan, W., Sun, G., Yin, L., Zhang, Z., and Tian, S. (2018). Ti₄O₇/g-C₃N₄ Visible light photocatalytic performance on hypophosphite oxidation: effect of annealing temperature. *Front. Chem.* 6, 37–47. doi: 10.3389/fchem.2018.00037
- Guo, J. S., and Sun, H. S. (2012). FePt nanoparticles assembled on graphene as enhanced catalyst for oxygen reduction reaction. *J. Am. Chem. Soc.* 134, 2492–2495. doi: 10.1021/ja2104334
- Guo, J. S., Zhang, S., Wu, H. L., and Sun, H. S. (2012). Co/CoO nanoparticles assembled on graphene for electrochemical reduction of oxygen. *Angew. Chem. Int. Ed.* 51, 11770–11773. doi: 10.1002/anie.201206152

DATA AVAILABILITY

The datasets generated for this study are available on request to the corresponding author.

AUTHOR CONTRIBUTIONS

The project is designed by PP. Scientific contributions in term of knowledge and discussion given by KV. SS and IH did the experimental work. DA and AD did the XPS analysis.

ACKNOWLEDGMENTS

This work was funded and supported by DST SERB, India (Grant no. EMR/2016/006050).

- Ikeda, T., Boero, M., Huang, F. S., Terakura, K., Oshima, M., and Ozaki, I. J. (2008). Carbon alloy catalysts: active sites for oxygen reduction reaction. *J. Phys. Chem. C* 112, 14706–14709. doi: 10.1021/jp806084d
- Jaouen, F., Proietti, E., Lefevre, M., Chenitz, R., Dodelet, J., Wu, P. G., et al. (2011). Recent advances in non-precious metal catalysis for oxygen-reduction reaction in polymer electrolyte fuel cells. *Energ. Environ. Sci.* 4, 114–130. doi: 10.1039/C0EE00011F
- Jiao, Y., Zheng, Y., Jaroniec, M., and Qiao, S. Z. (2014). Origin of the electrocatalytic oxygen reduction activity of graphene-based catalysts: a roadmap to achieve the best performance. *J. Am. Chem. Soc.* 136, 4394–4403. doi: 10.1021/ja500432h
- Kim, H., Lee, K., Woo, I. S., and Jung, Y. (2011). On the mechanism of enhanced oxygen reduction reaction in nitrogen-doped graphene nanoribbon. *Phys. Chem.* 13, 17505–17510. doi: 10.1039/c1cp21665a
- Kim, J., Lee, Y., and Sun, S. (2010). Structurally ordered Fe Pt nanoparticles and their enhanced catalysis for oxygen reduction reaction. *J. Am. Chem. Soc.* 132, 4996–4997. doi: 10.1021/ja1009629
- Lai, L., Potts, R. J., Zhan, D., Wang, L., Poh, K. C., Tang, C., et al. (2012). Exploration of the active center structure of nitrogen-doped graphene-based catalysts for oxygen reduction reaction. *Energ. Environ. Sci.* 5, 7936–7942. doi: 10.1039/c2ee21802j
- Li, H., Kang, W., Wang, L., Yue, Q., Xu, S., Wang, H., et al. (2013). Synthesis of three-dimensional flowerlike nitrogen-doped carbons by a copyrolysis route and the effect of nitrogen species on the electrocatalytic activity in oxygen reduction reaction. *Carbon* 54, 249–257. doi: 10.1016/j.carbon.2012.11.036
- Li, L., Xianghong, F., Yao, N., Siguo, C., Feng, S., Kun, X., et al. (2015). Insight into the effect of oxygen vacancy concentration on the catalytic performance of MnO₂. *ACS Catal.* 5, 4825–4832. doi: 10.1021/acscatal.5b00320
- Li, Y., Zhao, Y., Cheng, H., Hu, Y., Shi, G., Dai, L., et al. (2011). Nitrogen-doped graphene quantum dots with oxygen-rich functional groups. *J. Am. Chem. Soc.* 134, 15–18. doi: 10.1021/ja206030c
- Liang, Y., Li, Y., Wang, H., Zhou, G. J., Wang, and, J., and Dai, H. (2011). Co₃O₄ nanocrystals on graphene as a synergistic catalyst for oxygen reduction reaction. *J. Nat. Mater.* 10, 780–786. doi: 10.1038/nmat3087
- Liang, Y., Wang, H., Zhou, J., Li, Y., Wang, J., Regier, T., et al. (2012). Covalent hybrid of spinel manganese-cobalt oxide and graphene as advanced oxygen reduction electrocatalysts. *J. Am. Chem. Soc.* 134, 3517–3523. doi: 10.1021/ja210924t
- Liu, Q., and Zhang, J. (2013). Graphene supported Co-g-C₃N₄ as a novel metal-macrocylic electrocatalyst for the oxygen reduction reaction in fuel cells. *Langmuir* 29, 3821–3828. doi: 10.1021/la400003h
- Liu, R., Wu, D., Feng, X., and Mullen, K. (2010). Nitrogen-doped ordered mesoporous graphitic arrays with high electrocatalytic activity for oxygen reduction. *Angew. Chem. Int. Ed.* 122, 2619–2623. doi: 10.1002/ange.200907289

- Maheswari, N., and Muralidharan, G. (2015). Supercapacitor behaviour of cerium oxide nanoparticles in neutral aqueous electrolytes. *Energy Fuels* 29, 8246–8253. doi: 10.1021/acs.energyfuels.5b02144
- Maheswari, N., and Muralidharan, G. (2016). Hexagonal CeO₂ nanostructures: an efficient electrode material for supercapacitors. *Dalton Trans.* 45, 14352–14362. doi: 10.1039/C6DT03032G
- Niwa, H., Horiba, K., Harada, Y., Oshima, M., Ikeda, T., Terakura, K., et al. (2009). X-ray absorption analysis of nitrogen contribution to oxygen reduction reaction in carbon alloy cathode catalysts for polymer electrolyte fuel cells. *J. Power Sources* 187, 93–97. doi: 10.1016/j.jpowsour.2008.10.064
- Paraknowitsch, P. J., and Thomas, A. (2013). Doping carbons beyond nitrogen: an overview on advanced heteroatom doped carbons with boron, sulphur and phosphorus for energy applications. *Energy Environ. Sci.* 6, 2839–2855. doi: 10.1039/c3ee41444b
- Parvez, K., Yang, B. S., Hernandez, Y., Winter, A., Turchanin, A., Feng, L. X., et al. (2012). Nitrogen-doped graphene and its iron-based composite as efficient electrocatalysts for oxygen reduction reaction. *ACS Nano* 6, 9541–9550. doi: 10.1021/nn302674k
- Parwaiz, S., Bhunia, K., Das, A. K., Khan, M. M., and Pradhan, D. (2017). Cobalt-doped ceria/reduced graphene oxide nanocomposite as an efficient oxygen reduction reaction catalyst and supercapacitor material. *J. Phys. Chem. C* 121, 20165–20176. doi: 10.1021/acs.jpcc.7b06846
- Peng, Z. M., and Yang, H. (2009). Synthesis and oxygen reduction electrocatalytic property of Pt-on-Pd bimetallic heteronanostructures. *J. Am. Chem. Soc.* 131, 7542–7543. doi: 10.1021/ja902256a
- Perini, L., Durante, C., Favaro, M., Perazzolo, V., Agnoli, S., Granozzi, G., et al. (2015). Metal-support interaction in platinum and palladium nanoparticles loaded on nitrogen doped mesoporous carbon for oxygen reduction reaction. *ACS Appl. Mater. Interf.* 7, 1170–1179. doi: 10.1021/am506916y
- Qiao, X., Shijun, L., Guanghua, W., Ruiping, Z., Huiyu, S., and Xiuhua, L. (2016). Simultaneous doping of nitrogen and fluorine into reduced graphene oxide: a highly active metal-free electrocatalyst for oxygen reduction. *Carbon*, 2016. *Carbon* 99, 272–279. doi: 10.1016/j.carbon.2015.12.034
- Qu, L., Liu, Y., Baek, B. J., and Dai, L. (2010). Nitrogen-doped graphene as efficient metal-free electrocatalyst for oxygen reduction in fuel cells. *ACS Nano* 4, 1321–1326. doi: 10.1021/nn901850u
- Rao, V. C., Cabrera, R. C., and Ishikawa, Y. (2010). In Search of the active site in nitrogen-doped carbon nanotube electrodes for the oxygen reduction reaction. *J. Phys. Chem. Lett.* 1, 2622–2627. doi: 10.1021/jz100971v
- Raymundo-Piñero, E., Cazorla-Amoros, D., Linares-Solano, A., Find, J., Wild, U., and Schlögl, R. (2002). Structural characterization of N-containing activated carbon fibers prepared from a low softening point petroleum pitch and a melamine resin. *Carbon* 40, 597–608. doi: 10.1016/S0008-6223(01)00155-5
- Sharifi, T., Hu, G., Jia, X., and Wagberg, T. (2012). Formation of active sites for oxygen reduction reactions by transformation of nitrogen functionalities in nitrogen-doped carbon nanotubes. *ACS Nano* 6, 8904–8912. doi: 10.1021/nn302906r
- Sheng, H. Z., Shao, L., Chen, J. J., Bao, W. J., Wang, B. F., and Xia, H. X. (2011). Catalyst-free synthesis of nitrogen-doped graphene via thermal annealing graphite oxide with melamine and its excellent electrocatalysis. *ACS Nano* 5, 4350–4358. doi: 10.1021/nn103584t
- Soren, S., Bessoi, M., and Parhi, P. (2015). A rapid microwave initiated polyol synthesis of cerium oxide nanoparticle using different cerium precursors. *Ceram. Int.* 41, 8114–8118. doi: 10.1016/j.ceramint.2015.03.013
- Soren, S., Mohapatra, B. D., Mishra, S., Debnath, A. K., Aswal, D. K., Varadwaj, K. S. K., et al. (2016). Nano ceria supported nitrogen doped graphene as a highly stable and methanol tolerant electrocatalyst for oxygen reduction. *RSC Adv.* 6, 77100–77104. doi: 10.1039/C6RA13218A
- Sun, S., Xue, Y., Wang, Q., Li, S., Huang, H., Miao, H., et al. (2017). Electrocatalytic activity of silver decorated ceria microsphere for oxygen reduction reaction and its application in aluminium-air battery. *Chem. Comm.* 53, 7921–7924. doi: 10.1039/C7CC03691D
- Tan, H., and Ren, Z. (2016). Facile Synthesis of Co₃O₄/Nitrogen-doped graphene Composite with enhanced electrochemical performance. *Mater. Sci. Forum* 847, 14–21. doi: 10.4028/www.scientific.net/MSF.847.14
- Thomas, A., Fischer, A., Goettmann, F., Antonietti, M., Müller, J. O., Schlögl, R., et al. (2008). Graphitic carbon nitride materials: variation of structure and morphology and their use as metal-free catalysts. *J. Mater. Chem.* 18, 4893–4908. doi: 10.1039/b800274f
- Wang, H., Liang, Y., Li, G. Y., and Dai, J. H. (2011). Co_{1-x}S-graphene Hybrid: a high-performance metal chalcogenide electrocatalyst for oxygen reduction. *Angew. Chem. Int. Ed.* 50, 10969–10972. doi: 10.1002/anie.201104004
- Wang, N., Liu, J., Gu, W., Song, Y., and Wang, F. (2016). Toward synergy of carbon and La₂O₃ in their hybrid as efficient catalyst for oxygen reduction reaction. *RSC Adv.* 6, 77786–77795. doi: 10.1039/C6RA17104D
- Wang, S., Zhang, L., Xia, Z., Roy, A., D. W., Chang, J. B., et al. (2012). BCN graphene as efficient metal-free electrocatalyst for the oxygen reduction reaction. *Angew. Chem. Int. Ed.* 51, 4209–4212. doi: 10.1002/anie.201109257
- Wang, W., Song, J., Kang, Y., Chai, D., Zhao, R., and Lei, Z. (2017). Sm₂O₃ embedded in nitrogen doped carbon with mosaic structure: an effective catalyst for oxygen reduction reaction. *Energy* 133, 115–120. doi: 10.1016/j.energy.2017.05.095
- Wang, X., Maeda, K., Thomas, A., Takane, K., Xin, G., Carlsson, J. M., et al. (2009). A metal-free polymeric photocatalyst for hydrogen production from water under visible light. *Nat. Mater.* 8, 76–80. doi: 10.1038/nmat2317
- Wu, H. K., Zeng, Q., Zhang, B., Leng, X., Su, S. D., Gentle, R. I., et al. (2015). Structural origin of the activity in Mn₃O₄-graphene oxide hybrid electrocatalysts for the oxygen reduction reaction. *Chem. Sus. Chem.* 8, 3331–3339. doi: 10.1002/cssc.201500372
- Wu, Q., Jiang, M., Zhang, X., Cai, J., and Lin, S. (2017). A novel octahedral MnO/RGO composite prepared by thermal decomposition as a noble-metal free electrocatalyst for ORR. *J. Mater. Sci.* 52, 6656–6669. doi: 10.1007/s10853-017-0901-4
- Wu, X., Zhu, C., Wang, L., Guo, S., Zhang, Y., Li, H., et al. (2017). Control strategy on two-/four-electron pathway of water splitting by multidoped carbon based catalysts. *ACS Catal.* 3, 1637–1645. doi: 10.1021/acscatal.6b03244
- Xing, T., Zheng, Y., Li, H. L., Cowie, C. C. B., Gunzelmann, D., Qiao, S. Z., et al. (2014). Observation of active sites for oxygen reduction reaction on nitrogen-doped multilayer graphene. *ACS Nano* 8, 6856–6862. doi: 10.1021/nn501506p
- Xu, M., Han, L., and Dong, S. (2013). Facile fabrication of highly efficient g-C₃N₄/Ag₂O heterostructured photocatalysts with enhanced visible-light photocatalytic activity. *ACS Appl. Mater. Interf.* 5, 12533–12540. doi: 10.1021/am4038307
- Yan, H., Chen, Y., and Xu, S. (2012). Synthesis of graphitic carbon nitride by directly heating sulfuric acid treated melamine for enhanced photocatalytic H₂ production from water under visible light. *Int. J. Hydrogen Energy* 37, 125–133. doi: 10.1016/j.ijhydene.2011.09.072
- Yan, S. C., Li, Z. S., and Zou, Z. G. (2009). Photodegradation performance of g-C₃N₄ fabricated by directly heating melamine. *Langmuir* 25, 10397–10401. doi: 10.1021/la900923z
- Yang, Z., Yao, Z., Li, G., Fang, G., Nie, H., Liu, Z., et al. (2012). Sulfur-doped graphene as an efficient metal-free cathode catalyst for oxygen reduction. *ACS Nano* 6, 205–211. doi: 10.1021/nn203393d
- Zhang, C., Hao, R., Liao, H., and Hou, Y. (2013). Synthesis of amino-functionalized graphene as metal-free catalyst and exploration of the roles of various nitrogen states in oxygen reduction reaction. *Nano Energy* 2, 88–97. doi: 10.1016/j.nanoen.2012.07.021
- Zhang, J., and Song, C. (2008). Electrocatalytic oxygen reduction reaction, PEM fuel cell electrocatalysts and catalyst layers (Springer) 2008, 189–134. doi: 10.1007/978-1-84800-936-3
- Zhang, L., and Xia, Z. (2011). Mechanisms of oxygen reduction reaction on nitrogen-doped graphene for fuel cells. *J. Phys. Chem. C* 115, 11170–11176. doi: 10.1021/jp201991j
- Zhang, Y., Thomas, A., Antonietti, M., and Wang, X. C. (2008). Activation of carbon nitride solids by protonation: morphology changes, enhanced ionic conductivity, and photoconduction experiments. *J. Am. Chem. Soc.* 131, 50–51. doi: 10.1021/ja808329f

- Zheng, B., Wang, J., Wang, B. F., and Xia, H. X. (2013). Synthesis of nitrogen doped graphene with high electrocatalytic activity toward oxygen reduction reaction. *Electrochem. Commun.* 28, 24–26. doi: 10.1016/j.elecom.2012.11.037
- Zheng, Y., Jiao, Y., Zhu, Y., Cai, Q., Vasileff, A., Li, L. H., et al. (2017). Molecule-level g-C₃N₄ coordinated transition metals as a new class of electrocatalysts for oxygen electrode reactions. *J. Am. Chem. Soc.* 139, 3336–3339. doi: 10.1021/jacs.6b13100
- Zou, X., Su, J., Silva, R., Goswami, A., Sathe, B. R., and Asefa, T. (2013). Efficient oxygen evolution reaction catalyzed by low-density Ni-doped Co₃O₄ nanomaterials derived from metal-embedded graphitic C₃N₄. *Chem. Commun.* 49, 7522–7524. doi: 10.1039/c3cc42891e

Conflict of Interest Statement: The authors declare that the research was conducted in the absence of any commercial or financial relationships that could be construed as a potential conflict of interest.

Copyright © 2019 Soren, Hota, Debnath, Aswal, Varadwaj and Parhi. This is an open-access article distributed under the terms of the Creative Commons Attribution License (CC BY). The use, distribution or reproduction in other forums is permitted, provided the original author(s) and the copyright owner(s) are credited and that the original publication in this journal is cited, in accordance with accepted academic practice. No use, distribution or reproduction is permitted which does not comply with these terms.